Enhanced residual strains estimation in the annulus fibrosus through digital image correlation

Gilles Dusfour, Dominique Ambard, Patrick Cañadas, S. Lefloch

Enhanced residual strains estimation in the *annulus fibrosus* through digital image correlation.

G. Dusfour[1], D. Ambard[1], P. Cañadas[1], and S. Le Floc'h[1]

[1] LMGC, Univ. Montpellier, CNRS, Montpellier, France

Up-to-date, back pain is among the most prevalent health issues and generally takes its origins from lesions of the *annulus fibrosus* (AF). While the AF *ex vivo* mechanical properties are increasingly well understood, *in vivo* data are still missing. In particular, very few studies have precisely measured the residual strains within the AF and thus the *in vivo* deformation state of the AF is still miss-interpreted and miss-evaluated. In this work, we propose an original and robust method for the AF residual strains quantification via digital image correlation technics. Ten pig *annulus fibrosus* were extracted from adjacent vertebrae followed by a radial incision to release the residual strains. The operations were filmed and then analyzed by a custom digital image correlation software in order to quantify the circumferential, radial and shear residual deformations. Our results show that residual strains are of the same order of magnitude than the *in vivo* one. The average circumferential strains are in tension on the outer periphery ($[3.32; 5.94]\%$) and in compression on the inner periphery ($[-6.4; -1.69]\%$). The mean radial residual strains are essentially in compression ($[-10.4; 2.29]\%$). Locally, radial and circumferential residual strains can reach really large values up to 40% of compression. The mean shear strains remain very small ($-0.04\% \pm 2.88\%$). This study also shows that circumferential and radial residual strains evolve linearly along the radius and non-linearly along the angle. We propose a simple model to predict their spatial variations. Our results and methods will allow the quantification of more realistic *in vivo* strains and stresses within the human intervertebral disc.

Keywords annulus fibrosus ; soft tissue ; intervertebral disc; residual strain; mechanical characterization; growth; digital image correlation

1 Introduction

Back pains is the most common body location for health issues according to the work of (Breivik et al. 2006), which can lead in many cases to stop the profesional activity and causes psychological injuries like depression and anxiety (McWilliams et al. 2004). The origin of such pains is mainly due to deteriorated or herniated intervertebral disc (IVD) where the fribocartilaginous cells struggle to recreate annulus fibrosus (AF) tissue. However, the development of numerical models of the IVD which take into account the mechanical and nutritional properties allows to hypothesize differents scenarios of annulus fibrosus degeneration (Malandrino et al. 2011). While the *ex-vivo* mechanical behavior of the AF is well documented, the *in-vivo* mechanical state is only very little known. One of the crucial point to better modeled the *in-vivo* state is the accurate identification of the residual strain fields as it has already been done on arteries (Taber et al. 2001)

The most common technics to highlight residual strains is to realize one or several incisions within the tissue and to observe its opening. Once the tissue is fully open, the residual strains are estimated through the *opening angle method* (Fung 1984). Strong hypothesis are made on the roundness of the studied tissue which lead to global and sometimes poor estimations of the residual strain fields. Recently, (Sigaeva et al. 2019) intended to improve the *opening angle method* to apply it on different parts of the same tissue. Such an improvement allow to idealize the tissue in many cilyndrical shape and so to analyze residual strains for asymetric geometries. The residual strains and stresses estimations through radial incisions have been densely reported in the literature for cardiovascular tissues such as arteries and heart (Omens et al. 2003; Labrosse et al. 2013). But little is known on the residual strains in conjonctive tissues like the AF. To this date, only the work of (Michalek et al. 2012) and (Duclos et al. 2017) have intended to estimate the residual strains in the AF of bovine caudal IVDs. These two studies are based both on the *opening angle method* and the *arc lenght method* to obtain the circumferential strains whereas the radial strains are estimated by following the lamallae thickness evolution during the stress relaxation experiment. However, the global residual strains estimation of both of these studies are based on the roundness of the tissue, which make it difficult to reproduce on the more complex geometry of human AF. Therefore, we decided to realize a full field estimation of the residual strains through the digital image correlation (DIC) technics and to applied it to the more common pig models broadly used in the IVD biomechanics community (Busscher et al. 2010; Yingling et al. 1999).

Residual strains are present in a large variety of biological tissues both in animal and vegetal species (Goriely 2017). However, their genesis and purpose have not been clearly identified. Many authors

assumed differential growth within organs to be responsible of residual strains (Goriely 2017; Zahn et al. 2018). Others authors hypothesized a gradient in mechanical properties or in negatively charged molecules, as proteoglycans, to have a major role in the generation of residual strains and stresses (Azeloglu et al. 2008; Yang et al. 2018). For (Lanir 2009), residual strains and stresses are the results of all the previous combined mechanisms. Interestingly, residual strains in load bearing tissues seem to counterpart the load its support. Indeed, when biological tissues undergoing internal pressure, such as arteries, heart or annulus fibrosus, are cut in the radial direction they tend to open up (Fung 1991; Michalek et al. 2012; Duclos et al. 2017). Such residual strain or stress fields are assumed to create a homeostatic state of strain or stress in the loaded organs. This hypothesis led to the development of strain-induced growth laws to explain the pattern of residual strains in biological tissues (Taber et al. 2001).

Several growth models have been proposed in the literature to model the development of biological tissues (Goriely 2017; Ambrosi et al. 2002; Lubarda et al. 2002). Interestingly, most of these models have been applied to cardiovascular tissues. To this date no growth model of the intervertebral disc has been proposed. Moreover, very little authors have compared experimental residual strain fields to those obtain through simulation, excepting the work of (Taber et al. 2001). In order to completely model such complex phenomenon, anatomical, nutritional, mechanical and biological data are required and the results of the simulation finally need to be validatet. Many of the incoming data are available in the literature through the work of (Taylor 1975; Maroudas et al. 1975; Peacock 1951; Antoniou et al. 1996). Therefore, it is of crucial importance to accurately evaluate the residual strain fields to both validate and drive future IVD growth laws.

In this study, samples of pig annulus fibrosus were extracted from the adjacent vertebrae and cut in the radial direction. We propose a new method to measure residual strains regardless of the AF shape. The AF opening was recorded with a camera and analyzed through a dedicated DIC software to evaluate the residual strain fields in two dimensions. Novel data on the residual strains pattern are reported. We hypothesized that the AF display heterogeneous and anisotropic residual strain patterns dependent on both radius and angle. Moreover, it is assumed that the residual strains pattern can be modeled with a linear relationship with radius and non linear relationship with the angle.

2 Materials and methods

2.1 Specimen preparation

A total of ten annulus fibrosus sheets specimens were harvested from one large white pig spine of three month old (≈ 30 kg). Cervical, thoracic and lumbar spine have been extracted. The spine has been obtained from the local laboratory animal house and immediately frozen at -20°C. Prior to extracting the disc, the spinous and transverse processes were cut using a saw. The discs were separated from the adjacent vertebral bodies with a homemade double blade cutter to obtain a planar one millimeter thick annulus fibrosus sheet. Right after the extraction, the AF was cleaned with a physiological solution and graphite powder has been deposited to enhance the contrast. Next, all specimens were immersed in physiological solution of NaCl (9g/L) at 37°C and were cut along the radial direction on the lateral side with a surgical knife (Fig 1).

2.2 Numerical sample generation

For each experiments, a numerical geometry and a hexaedric mesh of the open sample were created with the GMSH mesh generator (Geuzaine et al. 2009). The boundaries of the numerical sample were defined manually to avoid any sides effects. For each sample, the center point of the nucleus pulposus was determined with contour detection using the *open cv*2 python library. This point allowed to compute an angle for each node of the mesh and to identified if the node belonged to the anterior [0° - 60°], lateral [60° - 120°] or posterior [120° - 180°] quadrant as illustrated on figure 2(b). This calculation can be extended for any division of the AF between two angles $[\alpha_{min}; \alpha_{max}]$. Such a division allows a refinement of the analysis. Finally, a thermal calculation allowed to compute a normalized radius as well as radial and circumferential direction for each node of the mesh (figs 2(a), 2(c), 2(d)).

2.3 Image analysis

2.3.1 Digital Image correlation

In order to estimate the residual strain fields, an iterative digital image correlation (DIC) technics has been implemented in *python* 2.7. For each sample, a total of 30 images were analysed with a mean number of 3480 ± 2427 correlation points. For each point, a subset dimension of 85x85 pixels^2 was searched in a 150x150 px^2 research area to identify both the displacement and the rotation of the subset. The research area in the deformed image was centered on the coordinates of the correlation point of the reference image. An initial angle interval of ±30° as been choosen. For each correlation point, if the correlation criterion (see eq. **??**) was higher than 0.9 the reference and deformed coordinates as well as the correlation

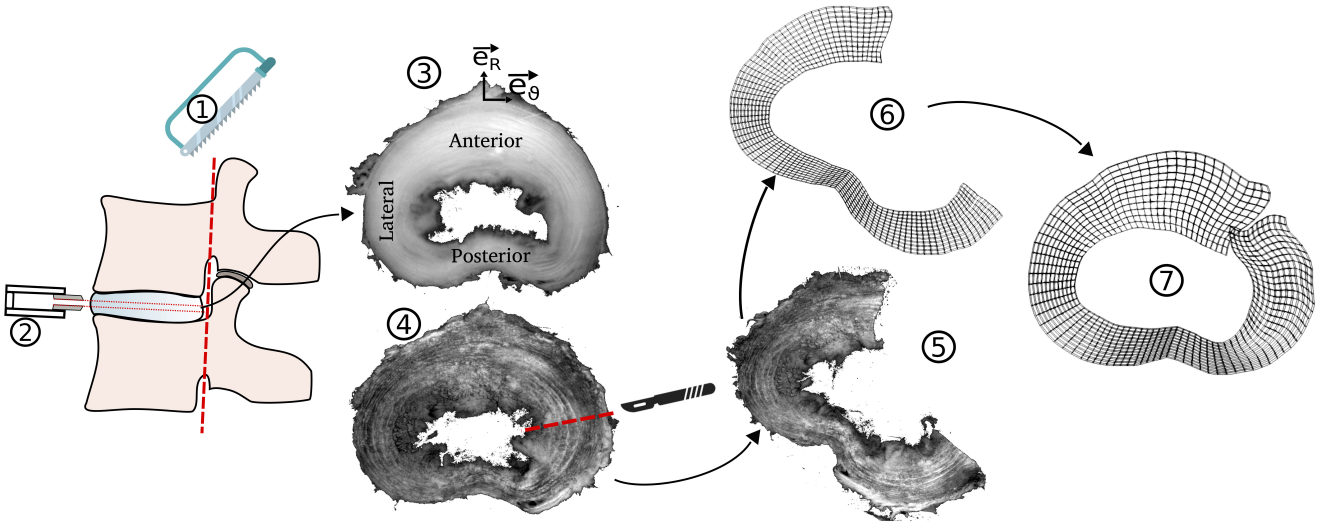

Figure 1: Schematic of the sheet specimen extraction protocol. Spinous and transverse processes are cut with a saw, sheet of annulus fibrosus is obtained with a homemade double blade cutter, outer and inner specimens are extracted with a surgical knife.

criterion and the rotation angle were saved in a results array. Otherwise, a next step of correlation was launched and an initial guess for the displacement and the rotation of the remaining points was computed using the mean displacement of the neighboring points already correlated. If needeed, angle interval was enlarged during the computation to maximized the correlation criterion.

2.3.2 Correlation criterion

The zero-normalizad cross-correlation criterion (ZNCC), as proposed by (Pan et al. 2009b), has been used to estimate the displacement of each point in between the reference image f and the deformed image g.

$$r_{ij} = \frac{\sum_{m\in M}\sum_{n\in N}[f(m,n)-\overline{f}][g(m+i,n+j)-\overline{g}]}{\sqrt{\sum_{m\in M}\sum_{n\in N}[f(m,n)-\overline{f}]^2}\sqrt{\sum_{m\in M}\sum_{n\in N}[g(m+i,n+j)-\overline{g}]^2}}$$

Where M and N are the x and y interval of the subset domain. The mean grayscale value of the reference and deformed image are respectively represent by $\overline{f}$ and $\overline{g}$. The displacement in the x and y direction are determined by :

$$(\Delta x, \Delta y) = argmax_{(ij)}\{r\} \tag{1}$$

2.3.3 Pointwise least square for strain estimation

In order to obtain full-field strain distribution from a noisy full-field displacement estimation, a pointwise local least-squares fitting technique has been used as proposed by (Wattrisse et al. 2001) and (Pan et al. 2009a). The implementation of this technique needs, for each node of the mesh, to create a circular window (arbitrary radius of 40 px) and to extract all the correlation points in the neighborhood. The displacement distribution in this window is then approximated as a linear plane :

$$\begin{aligned} u(i,j) &= a_0 + a_1 x + a_2 y \\ v(i,j) &= b_0 + b_1 x + b_2 y \end{aligned} \tag{2}$$

Where, u(i,j) and v(i,j) are the original horizontal and vertical displacements at pixel location (i,j). The least-squares method is then used to estimate the local unknown polynomial coefficients. Finally, the imposed displacement for each node of the hexaedric mesh is computed with identified polynomial coefficients and node coordinates. The strains are then computed at each Gauss Point element, through the derivative of the form function from the finite element technics, and extrapolate at node location.

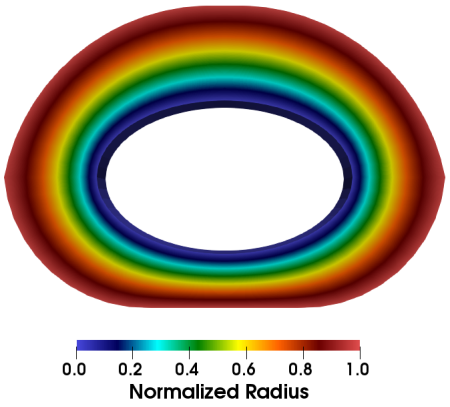

(a) Normalized radius

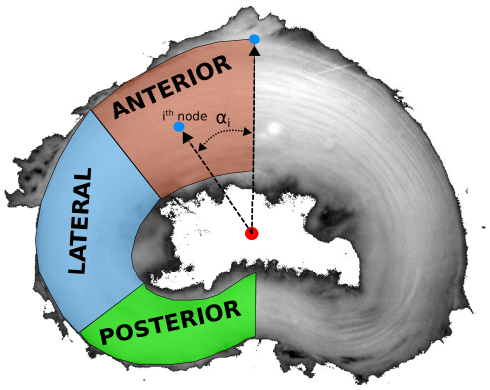

(b) Annulus zones

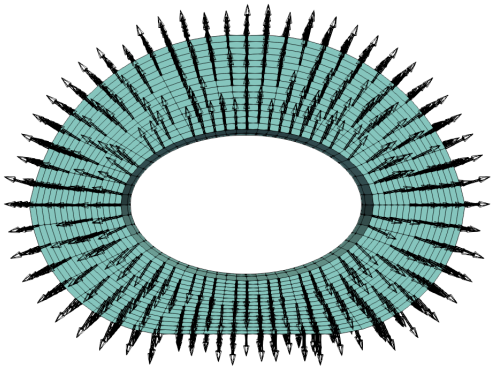

(c) Radial vectors

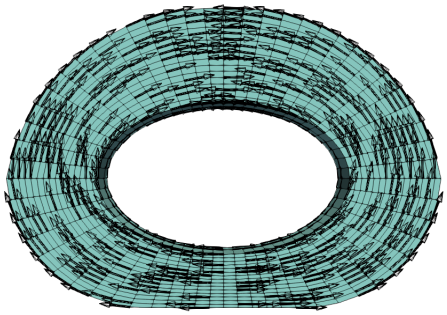

(d) Circumferential vector

2.4 Radial and circumferential strain field estimation

For each node of the final closed mesh, the Eulerian strain tensor $\underline{\underline{\boldsymbol{e}}}$ is projected on both radial ($\vec{\boldsymbol{e}}_{\boldsymbol{RR}}$) and circumferential($\vec{\boldsymbol{e}}_{\boldsymbol{\theta\theta}}$) directions to derive radial (e_{RR}), circumferential ($e_{\theta\theta}$) and shear strains ($e_{\theta R}$). With :

$$e_{\theta\theta} = \underline{\underline{\boldsymbol{e}}} : (\vec{\boldsymbol{e}}_{\boldsymbol{\theta\theta}} \otimes \vec{\boldsymbol{e}}_{\boldsymbol{\theta\theta}}) \tag{3}$$

$$e_{RR} = \underline{\underline{\boldsymbol{e}}} : (\vec{\boldsymbol{e}}_{\boldsymbol{RR}} \otimes \vec{\boldsymbol{e}}_{\boldsymbol{RR}}) \tag{4}$$

$$e_{\theta R} = \underline{\underline{\boldsymbol{e}}} : (\vec{\boldsymbol{e}}_{\boldsymbol{\theta\theta}} \otimes \vec{\boldsymbol{e}}_{\boldsymbol{RR}}) \tag{5}$$

With the aim to facilitate the reading of residual strain fields, graphics were created to visualize the average evolution of residual strain according to the normalized radius and area of study. Therefore, the radius was divided into twelve equal intervals with a $\frac{1}{12}$ step. For each radius interval $[r_{min}; r_{max}]$ and each zone interval $[\alpha_{min}; \alpha_{max}]$ median and interquartile range of residual strain were computed.

2.5 Residual strain model fitting

In order to take advantage of such a rich residual strain field, we derive a simple model to fully describe the residual strain state as function of the local coordinates. The heterogeneous residual strain pattern of the annulus fibrosus was modeled by a linear function of the normalized radius.

$$e_{\theta\theta}(r) = K_{\theta\theta}(\alpha) \times r + O_{\theta\theta}(\alpha) \tag{6}$$

$$e_{RR}(r) = K_{RR} \times r + O_{RR} \tag{7}$$

$$e_{\theta R}(r) = K_{\theta R} \times r + O_{\theta R} \tag{8}$$

Here K_{ii} is the gradient of residual strain along the normalized radius and O_{ii} the offset of the residual strain for the zero normalized radius. In order to respect the strain continuity in anterior and posterior area of the AF, the gradient $K_{\theta\theta}$ and the initial offset $O_{\theta\theta}$ of the circumferential strain were modeled as sum of *cosinus* functions with respect to the normalized angle:

$$K_{\theta\theta}(\alpha) = k + \sum_{i=1}^{n} A_i cos(i\alpha) \tag{9}$$

$$O_{\theta\theta}(\alpha) = k + \sum_{i=1}^{n} A_i cos(i\alpha) \tag{10}$$

Fitting was performed using *python* 2.7 and the $curve_fit$ function from the *scipy.optimize* library. The solution of the $curve\_fit$ function minimize the squared error between the predicted and the actual data.

The goodness of the fitting between the predicted and measured residual strain (e) was evaluated with the normalized root mean square error (NRMSE) :

$$NRMSE = \frac{\sqrt{\frac{\sum_{i=1}^{n}(e_i^{num} - e_i^{exp})^2}{n}}}{e_{max}^{exp} - e_{min}^{exp}} \times 100\% \tag{11}$$

2.6 Statistical analysis

The numerical data are presented as median ± interquartile range (IQR). All statistical analyses were performed at 95% confidence level using R statistical software. Nonparametric tests had to be applied because normality tests (Shapiro–Wilk) showed that all of the data groups do not have normal distributions. The studied values are the radial strain (e_{RR}), the circumferential strain ($e_{\theta\theta}$), the shear strain ($e_{\theta R}$), the gradient of each strain along the radius (K_{ii}) and the initial offset (O_{ii}). We performed a Kruskal-Wallis test to assess the dependence of the radial strain (e_{RR}), the circumferential strain ($e_{\theta\theta}$) and the shear strain ($e_{\theta R}$) on the normalized radius. Kruskal-Wallis test were also performed on the gradient of residual strain (K_{ii}) and on the initial offset (O_{ii}) to assess their dependence on the normalized angle.

3 Results

3.1 Qualitative method results

After the incision, all the samples open up to release the residual strains. These results highlight circumferential tension in the outer AF and compression in the inner AF. Figure 3 shows residuals strains fields for three different annulus fibrosus. Qualitatively, these results suggest that the strains fields are widely heterogeneous and anisotropic. Indeed the circumferential residual eulerian strains ($e_{\theta\theta}$) can exceed 15% both in tension and compression while the radial residual strains (e_{RR}) can reach 40% in compression but rarely goes into tension. Clearly, the radial (e_{RR}), circumferential ($e_{\theta\theta}$) and shear ($e_{R\theta}$) residual strains presents different pattern highlighting the anisotropic residual strain fields. Moreover, note that both circumferential ($e_{\theta\theta}$) and radial (e_{RR}) strains vary smoothly with radius and angle but also with disc level. Finally, the shape of final annulus fibrosus presented in figure 3 point out the DIC software issues to fully closed the incisions.

3.2 Comparison to literature

In order to facilitate the analysis and to compare it with the literature (Duclos et al. 2017), regional (anterior, lateral and posterior) variation along the normalized radius have been averaged and are presented in the figures 4(a), 4(c) and 4(b).

Fig 4(a) present the quantitative data of the circumferential ($e_{\theta\theta}$) residual strains along the normalized radius for the anterior, lateral and posterior regions. The exterior periphery ($r = 1$) is in tension with a more pronounced tensile state on the anterior and posterior quadrant than in the lateral quadrant (respectively 5.94% ± 1.54, 5.48% ± 3.06 and 3.32% ± 6.65). They gradually decrease along the radius to get closer to the zero strain state for the median radius ($r = 0.5$, respectively 2.26% ± 4.94%, −1.79% ± 5.56% and −0.12% ± 5.25%) and finally reach a global large compression state on the inner periphery ($r = 0$, respectively −6.4% ± 13.71%, −6.33% ± 11.09% ,−1.69% ± 9.24%). One can note the decreasing IQR with the increasing radius. Importantly, the Kruskall Wallis test showed that the circumferential ($e_{\theta\theta}$) are dependent on the normalized radius ($p < 0.001$).

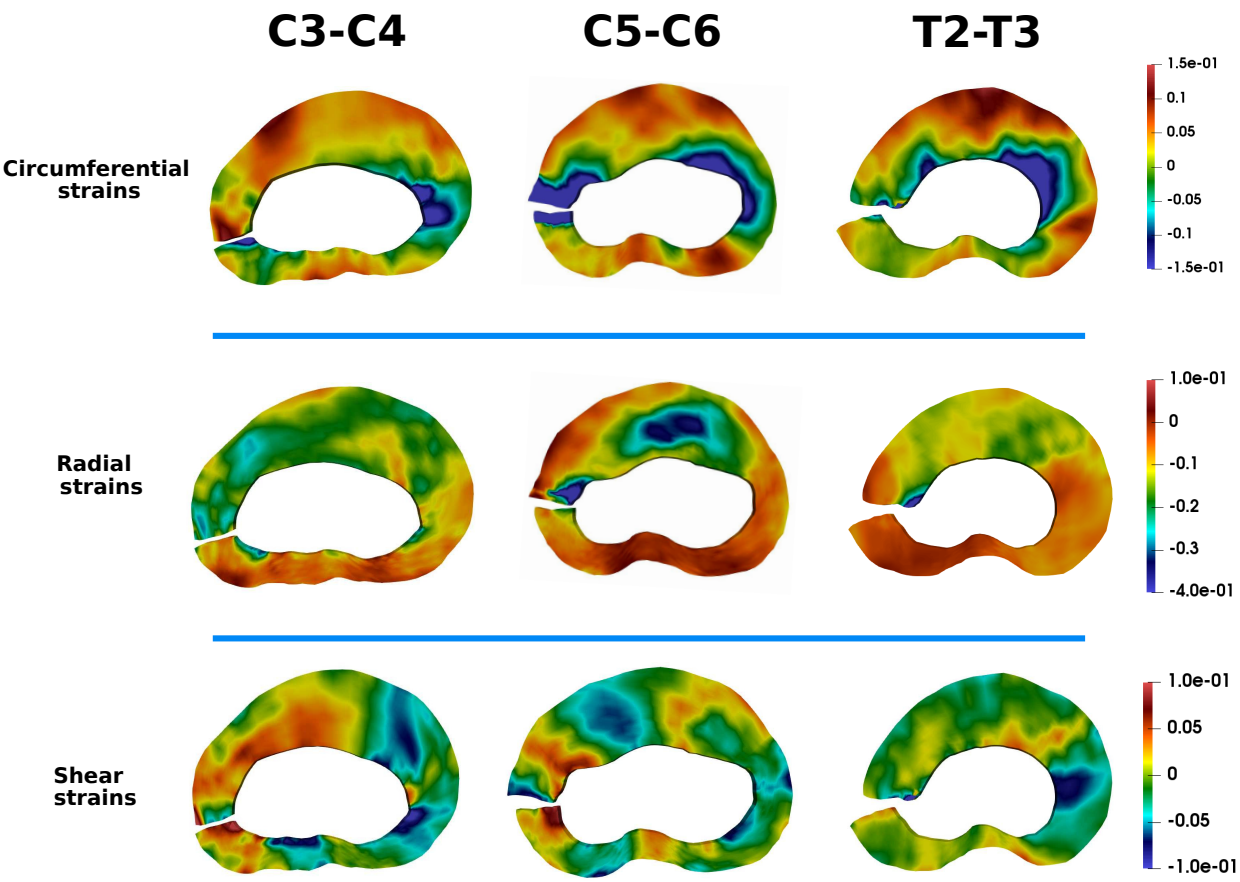

Figure 3: Circumferential, radial and shear residual strains fields for three annulus fibrosus.

Quantitative data of the radial (e_{RR}) and shear ($e_{R\theta}$) residual strains along the normalized radius are respectively presented in Fig.4(b) and Fig.4(c). Like the circumferential strains ($e_{\theta\theta}$), the Kruskall Wallis test showed that the radial strains (e_{RR}) are dependent on the normalized radius ($p < 0.05$) but not the shear residual strains ($e_{R\theta}$). The radial residual strains (e_{RR}) gradually increase in the anterior, lateral and posterior portions from the inner periphery ($r = 0$, respectively $-10.4\% \pm 9.79\%$, $-6.24\% \pm 10.75\%$,$-4.99\% \pm 5.55\%$) to the outer periphery ($r = 1$, respectively $-4.76\% \pm 9.07\%$, $-5.77\% \pm 5.33\%$ and $2.29\% \pm 4.97\%$). Finally, the shear residual strains ($e_{R\theta}$) is globally closed to the zero strain state ($-0.04\% \pm 2.88\%$).

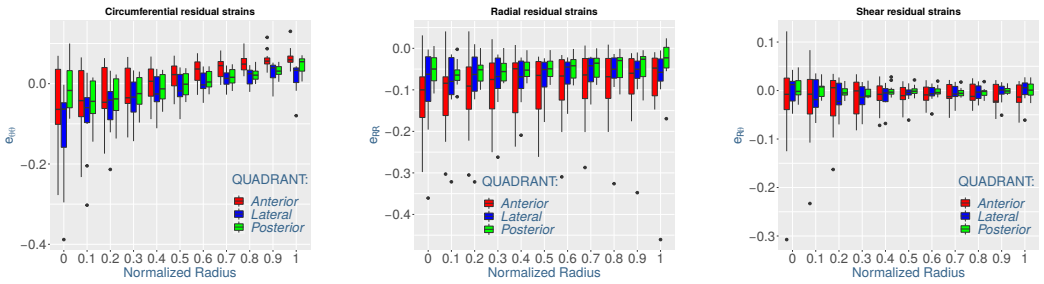

(a) circumferential strains **(b)** Radial strains. **(c)** Shear strains.

Figure 4: Residual strains in the annulus fibrosus along the normalized radius for the usual 3 different zones (anterior, lateral and posterior).

3.3 New local estimation of residual strain

3.3.1 Raw data

Nevertheless, the DIC method gives local estimates allowing to increase the number of studied portion with still a large amount of data. Such technics allows to identify significant differences between 15 different portions compartmentalized by angular interval of 12°, starting from the anterior side (0°-12°) and ending by the posterior side (168°-180°).

3.3.2 Linear model of residual strain

Figures 5(a),5(c) and 5(e) display the average of all AF residual circumferential, radial and shear strains fields on a idealized pig intervertebral disc. In additions to this, figures 5(b), 5(d) 5(f) shows overlays of experimental and model-predicted residual strains $e_{\theta\theta}$, e_{RR} and $e_{R\theta}$ versus the normalized radius (r) for 15 different portions and 10 radius values of the idealized pig annulus fibrosus. Note that the IQR are not presented to preserve the readability. For all the studied discs and zones, the prediction of the circumferential residual strains $e_{\theta\theta}$ give excellent results ($NRMSE = 12.54\% \pm 6.58\%$) while the prediction of the radial (e_{RR}) and shear ($e_{R\theta}$) strains are of poorer quality (respectively $NRMSE = 20.9\% \pm 7.74\%$ and $NRMSE = 21.2\% \pm 7.31\%$).

The first order polynomials model allow to obtain a gradient and an initial offset of residual strains along the normalized radius for 15 angular portions for all the studied discs. The evolution of the gradients (K_{ii}) and initial offsets (O_ii) with respect to the angle for the circumferential, radial and shear residuals strains are respectively presented in the figure 6(a),6(b), 6(c),6(d), 6(e),6(f) with a boxplot representation. While the circumferential gradient ($K_{\theta\theta}$) and initial offset ($O_{\theta\theta}$) evolve in a non linear way with both a peak centered on the [48°- 72°] interval, the radial and shear gradient (K_{RR}, $K_{R\theta}$) and initial offset (O_{RR}, $O_{R\theta}$) seem more stable with respect to the angle (α).

The results of the Kruskal Wallis test displayed that the circumferential strains gradient ($K_{\theta\theta}$) and the initial offset ($O_{\theta\theta}$) are dependent on the angular portion (respectively $p < 0.05$ and $p < 0.005$). The Wilcoxon test with a Bonferroni correction highlight that the gradient of the [48° - 60°] and [60° - 72°] portions are significantly higher than the gradient of the [144° - 156°]; [156° - 168°] and [168° - 180°] portions ($p < 0.05$). On the other hand the Kruskal Wallis test show that the gradient and initial offset of the radial (K_{RR}, O_{RR}) and shear ($K_{R\theta}$, $O_{R\theta}$) residual strains are not dependent on the angular portion ($p > 0.05$).

Therefore, the evolution of circumferential strains gradient ($K_{\theta\theta}$) and initial offset ($O_{\theta\theta}$) are respectively modeled with a triple and double sum of *cosinus* functions. The parameters of both fit functions are summarized in table 1. Both prediction of circumferential gradient and initial offset with respect to the angle give excellent results (respectively $NRMSE = 14.19\%$ and $NRMSE = 12.85\%$). Predictions of circumferential gradient and initial offset are plotted in figures 6(a) and 6(b). Regarding the non dependence on the angle of radial and shear strains gradient and initial offset, all of the data have been approximated with a single scalar also presented in table 1.

Parameters	A_1	A_2	A_3	k	NRMSE
$K_{\theta\theta}$	0.045	-0.024	-0.033	0.096	14.19%
$O_{\theta\theta}$	-0.031	0.051	-	-0.057	12.85%
K_{RR} = 0.012	-	-	-	-	36.88%
O_{RR} = -0.063	-	-	-	-	29.62%
$K_{R\theta}$ = 0.002	-	-	-	-	23.12%
$O_{R\theta}$ = -0.003	-	-	-	-	28.39%

Table 1: Values of polynomial parameters to describe the evolution of residual strains with respect to the normalized radius and angle.

Finally, the figure 7 exhibit the linear correlation between the residual strains gradients and the initial offset. Each point represents the residual strains gradient and the initial offset for a portion of a disc. This results establish that the greater the inner periphery is in compression the greater the gradient of residual strains along the normalized radius. (NRMSE : $\theta\theta = 7.47\%$; NRMSE : $RR = 6.88\%$; NRMSE : $R\theta = 7.47\%$)

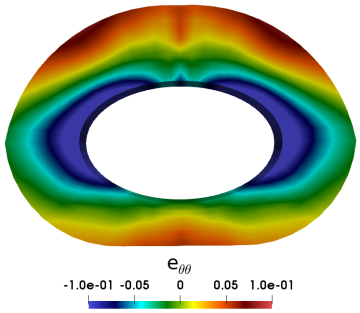

(a) Average circumferential strains field

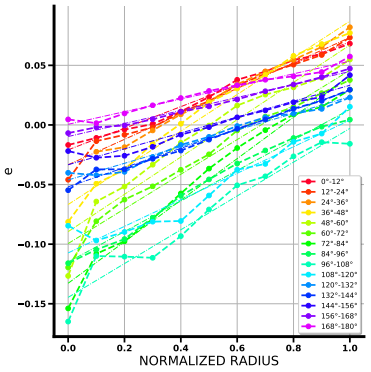

(b) Circumferential strains along the radius.

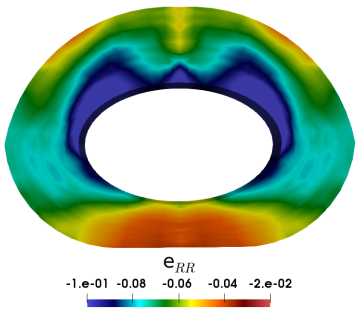

(c) Average radial strains field.

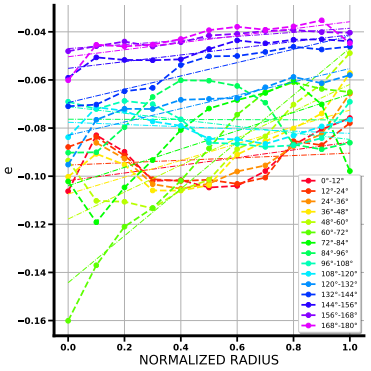

(d) Radial strains along the radius.

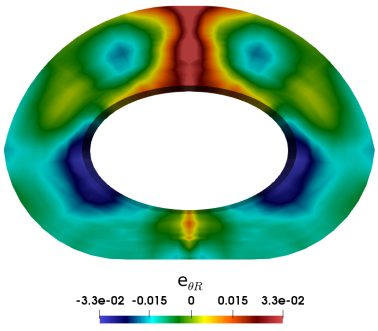

(e) Average shear strains field.

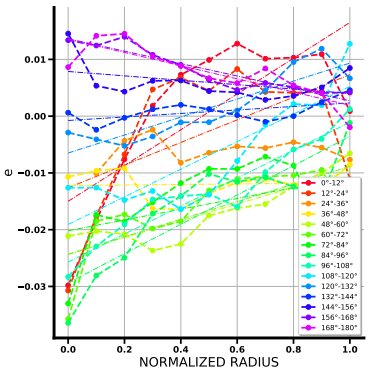

(f) Shear strains along the radius.

Figure 5: Projection of the average strains fields on a idealized AF and plot of residual strains along the normalized radius for all zones of the AF. In (b), (d) and (f), average experimental data are represented in dotted lines with circle markers and linear model fit in dotted lines.

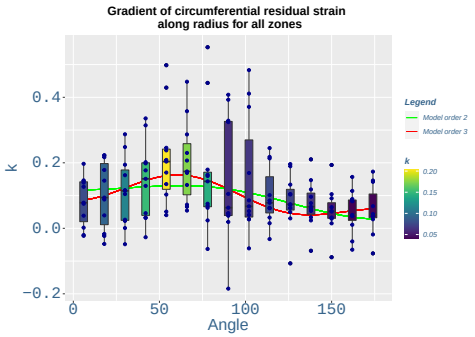

(a) circumferential residual strains gradient.

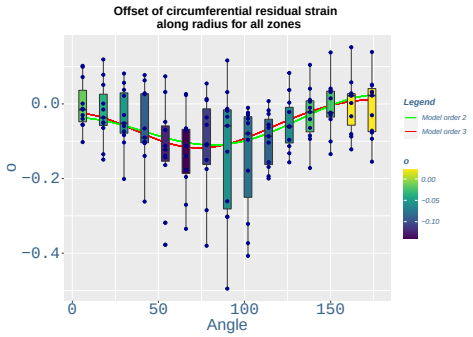

(b) circumferential residual strains offset.

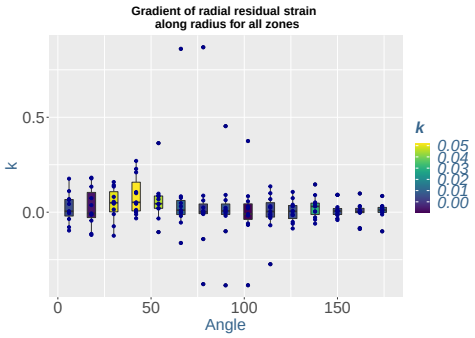

(c) Radial residual strains gradient.

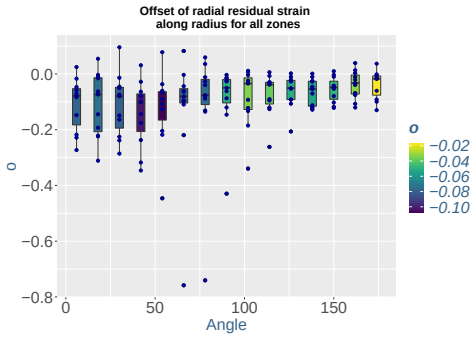

(d) Radial residual strains offset.

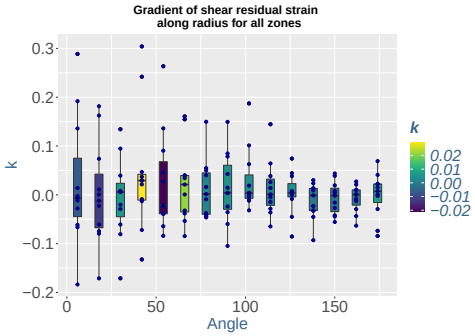

(e) Shear residual strains gradient.

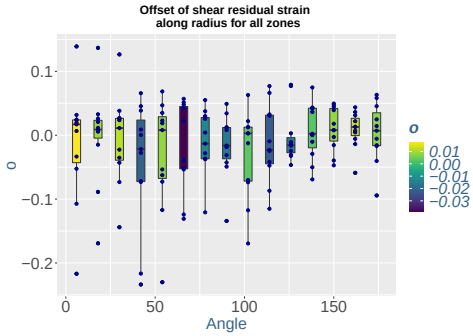

(f) Shear residual strains offset.

Figure 6: Boxplot of the residual strains gradients and initial offsets along the normalized radius in the circumferential, radial and shear directions. The results of the *cosinus* models are plot in (a) and (b), showing good agreement with the experimental data.

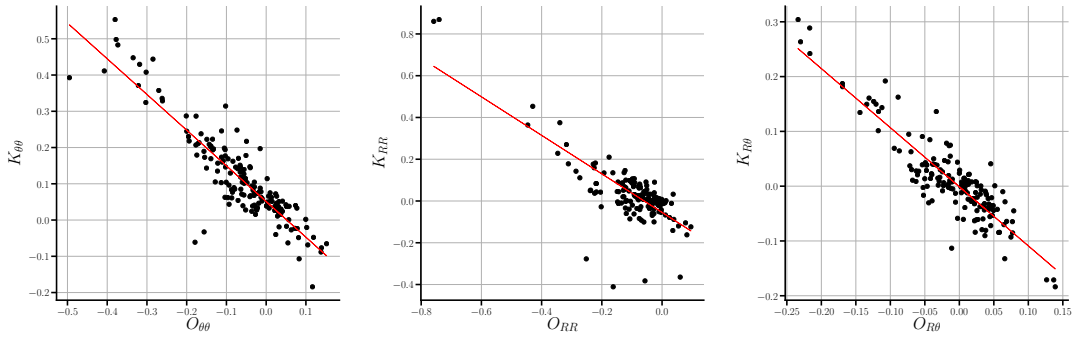

(a) circumferential strains. **(b)** Radial strains. **(c)** Shear strains.

Figure 7: Gradient of residual strains K_{ii} along the normalized radius with respect to the initial offset O_{ii} for each portions of AF of each disc.

4 Discussions

Our study aims to develop an original method to locally evaluate the residual strains of the pig annulus fibrosus through digital image correlation allowing full field evaluation. Following the spirit of (Fung 1991) and (Duclos et al. 2017) who respectively cut arteries and bovine AF in the radial direction to release the residual strains, our study realized similar experiments and for the first time to our knowledge used the digital image correlation method to locally estimate the circumferential ($e_{\theta\theta}$), radial (e_{RR}) and shear ($e_{R\theta}$) residual strains of the pig annulus fibrosus.

The work of (Michalek et al. 2012) and (Duclos et al. 2017), realized on bovines AF, display similar trends of the distribution of circumferential strains along the normalized radius except for the posterior region. Indeed, whereas the work of (Duclos et al. 2017) presents a minimum of the circumferential strains in the middle zone of the posterior region, our study show an monotonous increase from the inner to the outer zone of the AF whatever the regions. In our study the amplitude of compressive circumferential strain on the inner zone is twice as small as the results reported by (Duclos et al. 2017). Moreover, our results display a generalized state of compression in the radial direction which is not in accordance with the state of tension in the inner and middle zone presented by (Duclos et al. 2017). These large differences in both amplitude and state of deformation are probably due to the species of the extracted DIV. While our study has been realized on pig cervical, thoracic and lumbar AF, the studies of (Michalek et al. 2012) and (Duclos et al. 2017) have been done on bovine tail IVD. The residual strains present in these IVDs are convenient to analyze due to its roundness and availability but its gross morphology is different from the kidney shape of human and pig AF. However, despite similar gross morphology and mechanical behavior, human and pig IVD do not have equivalent dimensions and *in vivo* loading (Busscher et al. 2010; Beckstein et al. 2008). This put in evidence the necessity to evaluate the residual strain fields in the human AF. Therefore our robust methodology for the estimation of residual strains is of crucial importance regarding the kidney shape of the human AF.

Furthermore, this is the first time to our knowledge that shear residual strains of the AF are reported. Contrary to the circumferential and radial residual strains, the amplitude range of the shear residual strains is really small. The residual strain fields presented in this article as well as the evolution of residual strains along the radius highlight the relevance of studying the residual strains via the material directions of the AF. Indeed, at the same time the radial and tangential strains evolve in a smooth way along the normalized radius. On the contrary, this does not seem to be the case of shear strains. In addition, it has been shown that the residual strains evolve in a linear fashion along the normalized radius with good NRMSE [12% - 21%]. This made it possible to highlight significant differences between the various angular portions studied as well on the gradient as on the initial offset of the residual strains. In the case of circumferential strains, the evolution of the gradient and the initial offset are significantly dependent on the angle. Two lateral portions ([48°- 60°] and [60°- 72°]) have gradients significantly greater than the posterior portions ([144°- 156°], [156°- 168°] and [168°- 180°]), the gradients of which are the lowest in AF. The evolution of the gradients and the offsets of the radial and shears strains also evolve in a non-linear way but the lack of experiments does not allow to conclude to significant differences between portions.

Many numerical studies intend to predict the degeneration of the IVD by investigating the coupling between mechanical loading and biological properties (metabolic and nutrient transport, growth and remodeling through mechanostransduction) (Huang et al. 2008) and (Malandrino et al. 2011). While most of these studies used mechanical properties found experimentally, none of them took into account the residual strain and stress fields as initial conditions of the numerical models. Our results display a large amplitude of the medial residual strains distribution along the normalized radius (circumferential : [-6.4% ;

6%], radial : [-10.4%;2.29%] and shear : [-0.04% ± 2.88%]) which could greatly influence the computed global mechanical response as well as the nutrient transport. Such identified residual strain fields would reduced the hoop strains and stresses in the inner periphery of the loaded AF. In consequence, it would tend to homogeneize the circumferential strains along the normalized radius during normal loading. On another hand, the experimental studies of (O'Connell et al. 2007), (O'connell et al. 2011) and (Tsantrizos et al. 2005) found that the AF, whatever the regions, is in a radial tensile state when the entire IVD is loaded under compression, flexion or lateral bending. Moreover, the numerical study of (Yang et al. 2018) show large radial strains due to the swelling properties developed by the high glycosaminoglycan content. Therefore, the radial residual strains would tend to decrease the global radial strain state generated by both mechanical and chemical loads. In regards to all these features, it would be interesting to integrate an initial residual strain fields in numerical studies by using the multiplicative decomposition of the deformation gradient, as proposed by (Pena et al. 2006; Rausch et al. 2013; Balzani et al. 2006), and to compute its influence on the mechanical and nutrient transport fields. Therefore, we proposed a simple *cosinus* sum function model based on normalized radius and angle to fully describe the residual strain state within the IVD. Finally, in addition to the homogenization of the *in vivo* strains and stresses of the AF, the residual strains could also contribute to increase the global stiffness of the vertebral column.

The origins of such residual strain fields are still under debate, does it come from a gradient in glycosaminoglycan or a gradient in growth? While our results in the circumferential direction are equivalent to those induced by the osmotic pressure in the study of (Yang et al. 2018), those in the radial direction are completely different. These large discrepancies highlight the fact that residual strains do not arise only from the osmotic pressure but also from others phenomenons such as growth and remodeling. However, it seems difficult to segregate the impact of osmotic pressure from the growth and remodeling process. Indeed, during the growth and remodeling process both collagen proteins and glycosaminoglycan are secreted. While the new created matter will exert forces on the old one, the new glycosaminoglycan will increase the negative charged density of the annulus fibrosus and thus increased the osmotic pressure. One possible way to determine the impact of glycosaminoglycan distribution would be to realize residual strains relaxation in hypertonic and hypotonic conditions as it has already been done on arteries by (Azeloglu et al. 2008). We realized some preliminaries experiments by modifying the NaCl bath from a isotonic saline (9g/L) to a hypertonic saline (100g/L). Contraction under 2% in the radial direction and dilatation up to 2% in the circumferential direction were observed. These preliminaries results suggest that charged effect are of minor importance in residual strains genesis but further studies are needed to fully understand this phenomenon. It is now of crucial importance to develop growth models which take into account both the multiplicative decomposition of the gradient of the deformation but also the creation of new negative charge (Armstrong et al. 2016). Finally, the strong linear correlation between the level of residual strains on the inner periphery and the gradient of these same strains along the normalized radius (fig 7) exhibit the spatial interdependence of the residual strains. Such a phenomenon could be a key point for the understanding of growth pattern and the development of new IVD growth law.

One major limitation of our work is the impossibility to determine residual strains in the axial direction. One could develop an experimental setup with a stereo-correlation techniques to determine the strains in the axial direction. It could also be relevant to develop a adapted white and black powder to optimize the speckle pattern and thus greatly refine the digital image correlation results. The use of such a powder could also allow a more detailed study of the tensile test sample as well as the analysis of failure mechanisms of the *annulus fibrosus*. Finally, as (Lee et al. 2020) points out, most of the studies on residual strains focuses on the continuous scale whereas the microscopic scale seems essential. Therefore, future studies should combine the relaxation of residual strains by the radial incision technique and the microscopic study of the *annulus fibrosus*.

5 Conclusion

By combining differents methods, radial incision and digital image correlation, this study highlights the complex residual strain fields in the *annulus fibrosus*. Especially a strong and zone dependent circumferential residual strain gradient along the normalized radius and stable and strong radial compressive strains. This exhibit that our DIC technique is a robust tool for the characterization of the residual strains on the *annulus fibrosus* and that it could be apply on human samples. Our study shows that numerical models of the AF should integrate residual strains to better mimick the *in vivo* behavior of the IVD. Finaly, we hope that our work will deepen our understanding on the origin and the characterization of residual strains.

Bibliographic References

Ambrosi, D and F Mollica (2002). "On the mechanics of a growing tumor". *International journal of engineering science* 40.12, pp. 1297–1316

Antoniou, J., T. Steffen, F. Nelson, N. Winterbottom, A. P. Hollander, R. A. Poole, M. Aebi, and M. Alini (1996). "The human lumbar intervertebral disc: evidence for changes in the biosynthesis and denaturation of the extracellular matrix with growth, maturation, ageing, and degeneration." *Journal of Clinical Investigation* 98.4, p. 996

Armstrong, M. H., A. B. Tepole, E. Kuhl, B. R. Simon, and J. P. V. Geest (2016). "A finite element model for mixed porohyperelasticity with transport, swelling, and growth". *PloS one* 11.4, e0152806

Azeloglu, E. U., M. B. Albro, V. A. Thimmappa, G. A. Ateshian, and K. D. Costa (2008). "Heterogeneous transmural proteoglycan distribution provides a mechanism for regulating residual stresses in the aorta". *American Journal of Physiology-Heart and Circulatory Physiology* 294.3, H1197–H1205

Balzani, D., J. Schröder, and D. Gross (2006). "Simulation of discontinuous damage incorporating residual stresses in circumferentially overstretched atherosclerotic arteries". *Acta Biomaterialia* 2.6, pp. 609–618

Beckstein, J. C., S. Sen, T. P. Schaer, E. J. Vresilovic, and D. M. Elliott (2008). "Comparison of animal discs used in disc research to human lumbar disc: axial compression mechanics and glycosaminoglycan content". *Spine* 33.6, E166–E173

Breivik, H., B. Collett, V. Ventafridda, R. Cohen, and D. Gallacher (2006). "Survey of chronic pain in Europe: prevalence, impact on daily life, and treatment". *European journal of pain* 10.4, pp. 287–333

Busscher, I., J. J. Ploegmakers, G. J. Verkerke, and A. G. Veldhuizen (2010). "Comparative anatomical dimensions of the complete human and porcine spine". *European Spine Journal* 19.7, pp. 1104–1114

Duclos, S. E. and A. J. Michalek (2017). "Residual strains in the intervertebral disc annulus fibrosus suggest complex tissue remodeling in response to in-vivo loading". *Journal of the Mechanical Behavior of Biomedical Materials* 68, pp. 232–238

Fung, Y. (1984). "What principle governs the stress distribution in living organs?" *Biomechanics in China, Japan and USA*, pp. 1–13

Fung, Y. (1991). "What are the residual stresses doing in our blood vessels?" *Annals of biomedical engineering* 19.3, pp. 237–249

Geuzaine, C. and J.-F. Remacle (2009). "Gmsh: A 3-D finite element mesh generator with built-in pre-and post-processing facilities". *International journal for numerical methods in engineering* 79.11, pp. 1309–1331

Goriely, A. (2017). *The mathematics and mechanics of biological growth*. Vol. 45. Springer

Huang, C.-Y. and W. Y. Gu (2008). "Effects of mechanical compression on metabolism and distribution of oxygen and lactate in intervertebral disc". *Journal of biomechanics* 41.6, pp. 1184–1196

Labrosse, M. R., E. R. Gerson, J. P. Veinot, and C. J. Beller (2013). "Mechanical characterization of human aortas from pressurization testing and a paradigm shift for circumferential residual stress". *Journal of the mechanical behavior of biomedical materials* 17, pp. 44–55

Lanir, Y. (2009). "Mechanisms of residual stress in soft tissues". *Journal of biomechanical engineering* 131.4, p. 044506

Lee, T., M. A. Holland, J. Weickenmeier, A. K. Gosain, and A. B. Tepole (2020). "The geometry of incompatibility in growing soft tissues: Theory and numerical characterization". *Journal of the Mechanics and Physics of Solids*, p. 104177

Lubarda, V. A. and A. Hoger (2002). "On the mechanics of solids with a growing mass". *International journal of solids and structures* 39.18, pp. 4627–4664

Malandrino, A., J. Noailly, and D. Lacroix (2011). "The effect of sustained compression on oxygen metabolic transport in the intervertebral disc decreases with degenerative changes". *PLoS computational biology* 7.8, e1002112

Maroudas, A, R. Stockwell, A Nachemson, and J Urban (1975). "Factors involved in the nutrition of the human lumbar intervertebral disc: cellularity and diffusion of glucose in vitro." *Journal of anatomy* 120.Pt 1, p. 113

McWilliams, L. A., R. D. Goodwin, and B. J. Cox (2004). "Depression and anxiety associated with three pain conditions: results from a nationally representative sample". *Pain* 111.1-2, pp. 77–83

Michalek, A., M. Gardner-Morse, and J. Iatridis (2012). "Large residual strains are present in the intervertebral disc annulus fibrosus in the unloaded state". *Journal of biomechanics* 45.7, pp. 1227–1231

O'Connell, G. D., W. Johannessen, E. J. Vresilovic, and D. M. Elliott (2007). "Human internal disc strains in axial compression measured noninvasively using magnetic resonance imaging". *Spine* 32.25, pp. 2860–2868

O'connell, G. D., E. J. Vresilovic, and D. M. Elliott (2011). "Human intervertebral disc internal strain in compression: the effect of disc region, loading position, and degeneration". *Journal of Orthopaedic Research* 29.4, pp. 547–555

Omens, J., A. McCulloch, and J. Criscione (2003). "Complex distributions of residual stress and strain in the mouse left ventricle: experimental and theoretical models". *Biomechanics and modeling in mechanobiology* 1.4, pp. 267–277

Pan, B., A. Asundi, H. Xie, and J. Gao (2009a). "Digital image correlation using iterative least squares and pointwise least squares for displacement field and strain field measurements". *Optics and Lasers in Engineering* 47.7-8, pp. 865–874

Pan, B., K. Qian, H. Xie, and A. Asundi (2009b). "Two-dimensional digital image correlation for in-plane displacement and strain measurement: a review". *Measurement science and technology* 20.6, p. 062001

Peacock, A (1951). "Observations on the pre-natal development of the intervertebral disc in man". *Journal of anatomy* 85.Pt 3, p. 260

Pena, E, M. Martinez, B Calvo, and M Doblaré (2006). "On the numerical treatment of initial strains in biological soft tissues". *International Journal for Numerical Methods in Engineering* 68.8, pp. 836–860

Rausch, M. K. and E. Kuhl (2013). "On the effect of prestrain and residual stress in thin biological membranes". *Journal of the Mechanics and Physics of Solids* 61.9, pp. 1955–1969

Sigaeva, T., E. Di Martino, and M. Destrade (2019). "Multisector method for arteries: The residual stresses of circumferential rings with non-trivial openings". *arXiv preprint arXiv:1901.06848*

Taber, L. A. and J. D. Humphrey (2001). "Stress-modulated growth, residual stress, and vascular heterogeneity". *Journal of biomechanical engineering* 123.6, pp. 528–535

Taylor, J. (1975). "Growth of human intervertebral discs and vertebral bodies." *Journal of Anatomy* 120.Pt 1, p. 49

Tsantrizos, A., K. Ito, M. Aebi, and T. Steffen (2005). "Internal strains in healthy and degenerated lumbar intervertebral discs". *Spine* 30.19, pp. 2129–2137

Wattrisse, B, A Chrysochoos, J.-M. Muracciole, and M Némoz-Gaillard (2001). "Analysis of strain localization during tensile tests by digital image correlation". *Experimental Mechanics* 41.1, pp. 29–39

Yang, B. and G. D. O'Connell (2018). "GAG content, fiber stiffness, and fiber angle affect swelling-based residual stress in the intact annulus fibrosus". *Biomechanics and modeling in mechanobiology*, pp. 1–14

Yingling, V. R., J. P. Callaghan, and S. M. McGill (1999). "The porcine cervical spine as a model of the human lumbar spine: an anatomical, geometric, and functional comparison." *Journal of Spinal Disorders* 12.5, pp. 415–423

Zahn, A. and D. Balzani (2018). "A combined growth and remodeling framework for the approximation of residual stresses in arterial walls". *ZAMM-Journal of Applied Mathematics and Mechanics/Zeitschrift für Angewandte Mathematik und Mechanik* 98.12, pp. 2072–2100